

## Microstructure and fracture toughness of a TiAl–Nb composite consolidated by spark plasma sintering

YANG Xin<sup>1,2</sup>, XI Zheng-ping<sup>1,2</sup>, LIU Yong<sup>1</sup>, TANG Hui-ping<sup>2</sup>, HU Ke<sup>3</sup>, JIA Wen-peng<sup>2</sup>

1. State Key Laboratory of Powder Metallurgy, Central South University, Changsha 410083, China;
2. State Key Laboratory of Porous Metal Materials, Northwest Institute for Nonferrous Metal Research, Xi'an 710016, China;
3. National Engineering Research Center of Near-Net-Shape Forming for Metallic Materials, South China University of Technology, Guangzhou 510641, China

Received 6 March 2012; accepted 24 October 2012

**Abstract:** A TiAl–Nb composite was prepared by spark plasma sintering (SPS) at 1250 °C and 50 MPa for 5 min from prealloyed TiAl powder and elemental Nb powder in a molar ratio of 9:1 for improving the fracture toughness of TiAl alloy at room temperature. The microstructure, phase constitute, fracture surface and fracture toughness were determined by X-ray diffractometry, electron probe micro-analysis, scanning and transmission electron microscopy and mechanical testing. The results show that the sintered samples mainly consist of  $\gamma$  phase, O phase, niobium solid solution (Nbss) phase and B2 phase. The fracture toughness is as high as 28.7 MPa·m<sup>1/2</sup> at room temperature. The ductile Nbss phase plays an important role in absorbing the fracture energy in front of the cracks. Moreover, B2 phase can branch the propagation of the cracks. The microhardness of each phase of the composite was also tested.

**Key words:** TiAl–Nb composite; fracture; spark plasma sintering (SPS); powder metallurgy; fracture toughness; fracture energy; crack propagation

### 1 Introduction

TiAl alloy and TiAl-based composite have great potential for applications as the next generation of elevated-temperature structure materials, mainly due to their high specific strength and high temperature resistance [1–5]. However, the application of gamma TiAl is still limited, partly due to its low toughness at room temperature. The fracture toughness of brittle materials can be improved by incorporating ductile reinforcement [6]. One approach is known as ductile phase toughening; another approach is to reduce the grain size [7]. Experimental investigations have demonstrated that considerable toughening of some systems consisting of brittle matrix has been achieved by incorporating a ductile phase, such as Al<sub>2</sub>O<sub>3</sub>–Al [8], WC–Co [9], and NbSi<sub>10</sub>–Nb [10]. In these systems, the plastic stretching of the ductile phase which bridges advancing cracks in the brittle matrix reduces the crack

tip stress to yield an increment in toughness over the matrix. The phase diagram of the TiAl–Nb system indicates that this system can offer a type of microstructure to enable TiAl–Nb composite containing O phase (based on Ti<sub>2</sub>AlNb), niobium solid solution (Nbss) phase and B2 phase. The Nbss phase behaves in a ductile manner and provides significant toughening of the TiAl matrix, and alloys with a significant volume fraction of O and B2 phases have shown excellent creep resistance combined with some room temperature ductility from the existence of multiple slip systems [11]. The room-temperature fracture toughness of the composite is sensitive to the volume fraction of constituent phase as well as to the microstructure.

Spark plasma sintering (SPS), a novel powder metallurgy (PM) technology, to enhance the mechanical properties of TiAl alloys, is regarded as a rapid sintering densification process allowing sintering at lower temperature for a shorter soaking time, which can preserve the characteristics of original interface of the

sample [12–16]. Therefore, SPS process was employed as a key process to synthesize the composite. To the best of our knowledge, an understanding of the effect of Nb on the fracture toughness of TiAl based composite has less been reported. The purpose of this work is to investigate the microstructure and fracture toughness at room temperature of TiAl–Nb composite consolidated by SPS.

## 2 Experimental

The starting materials were commercially available elemental Nb powders, and pre-alloyed powder with a nominal composition of Ti–47Al–2Cr–2Nb–0.2W (mole fraction, %) prepared by plasma rotating electrode processing. The powders with a mole ratio of TiAl to Nb of about 9:1 were firstly mixed, and then filled into a graphite die which was moved into a SPS furnace of DR. SINTERING–8250 mode. In order to avoid overheating, the powder compact was heated first to 1150 °C at 100 °C/min, heated to 1200 °C at 50 °C/min, followed by heating to 1250 °C at 25 °C/min, kept at the designed temperature for 5 min and last cooled in the furnace. Figure 1 shows three curves of the processing parameters, such as sintering temperature, current and relative displacement of the punches, as a function of time. The relative displacement of the punch is expressed in percentage of the maximum of initial powders compact. The temperature curve displays the variation measured by the external pyrometer over 600 °C. For this explanation, the selected holding temperature was 1250 °C. A uniaxial pressure of 50 MPa was applied to the compact powders in the whole duration. Figure 1 shows three main ranges for the displacement variation and a remarkable fluctuation for the current, which should be interpreted as follows. During the initial current increasing, the powder is compressed as a green body with a high porosity by pressure. This is followed by a density increasing stage with increasing the current.

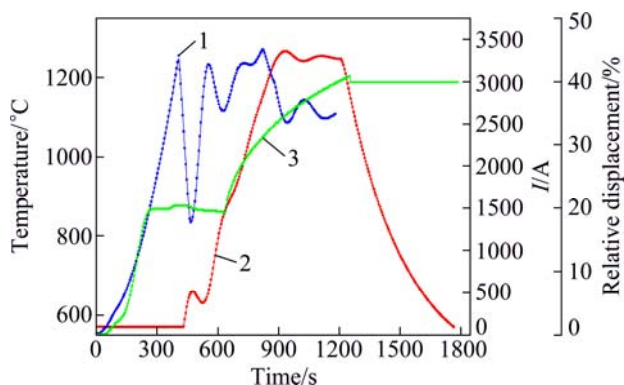


Fig. 1 Temperature, current and relative displacement of punch as function of time performed at 1250 °C for TiAl–Nb powder: 1—Current; 2—Temperature; 3—Relative displacement

Sparking occurs in the plateau-like stage as the temperature reaches about 650 °C under 50 MPa. Sintering begins in the last stage as the temperature reaches about 850 °C. Under these conditions, the pressure exceeds the yield stress at a temperature above the brittle–ductile transition. The sintered samples were cylinder disks with a diameter of 30 mm and a thickness of 6–7 mm was obtained in 30 min.

The density was measured by the Archimedes method. The phase composition and fracture surface were characterized by X-ray diffraction (XRD), electron probe micro-analysis (EMPA), scanning electron microscopy (SEM) and transmission electron microscopy (TEM). The grain size was measured by mean linear intercept method. The lamellar spacing given in this work was arithmetic average value measured without taking account of type of lamellar boundaries. The TEM foils of TiAl were prepared by standard twin jet electropolishing at 15 V and –30 °C.

Fracture toughness specimens with dimensions of 3 mm × 6 mm × 24 mm were cut from the sintered pancake by an electro-discharge machine, and then mechanically polished using SiC paper and Al<sub>2</sub>O<sub>3</sub> particles with water. A single notch with about 3 mm in length was introduced halfway along the length by EDM wire with 0.1 mm in diameter, without pre-cracking. The tests were executed at an initial cross-head speed of 0.5 mm/min in a three-point bending manner. The values of  $K_Q$  of fracture specimens were calculated by the following formulas [17]:

$$S = 4W, K_Q = \left( \frac{SP_q}{BW^{3/2}} \right) Y_{(a/w)} \quad (1)$$

$$Y_{(a/w)} = 3(a/w)^{1/2} \{1.99 - (a/w)(1 - a/w) \cdot [2.15 - 3.93(a/w) + 2.7(a/w)^2] \} / [2(1 + a/w)(1 - a/w)^{3/2}] \quad (2)$$

where  $K_Q$  is the stress intensity factor for specimen;  $W$  is the width of specimen;  $B$  is the thickness of specimen;  $a$  is the length of the slit notch;  $S$  is the span of the loading;  $Y_{(a/w)}$  is the related coefficient;  $P_q$  is measured by load–displacement curve according to standard GB/T 4161–1984. The micro-hardness values of different phases of the samples were determined by nanoindentation at room temperature.

## 3 Results and discussion

### 3.1 Microstructure

The density of the spark plasma sintered sample is 4.46 g/cm<sup>3</sup>, almost fully dense compared with the theoretical density of this composition, 4.48 g/cm<sup>3</sup>. There is not any pore defect in the samples according to the

EMPA images. XRD pattern in Fig. 2 shows that under the sintering condition, the microstructure consists of five phases:  $\gamma$ -TiAl ( $L1_0$ ), O, B2, Nbss and  $\alpha_2$ -Ti<sub>3</sub>Al ( $D0_{19}$ ). The semi-quantitative calculations show the volume fractions are about 55%, 19%, 16%, 8% and 2%, respectively. This suggests that the mixed powder has experienced a complex reaction and a lot of non-equilibrium phases retains during SPS.

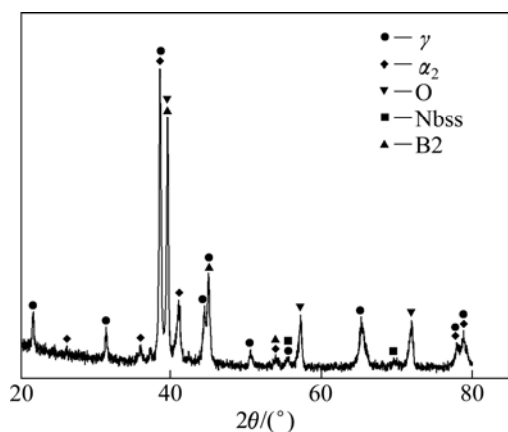


Fig. 2 XRD pattern of TiAl-Nb composite

EMPA of the as-sintered composite is shown in Fig. 3(a). The dendritic gray grains are Ti<sub>2</sub>AlNb containing O/B2 alternate phase structure (marked A), the dark grains are lamellar colonies containing  $\gamma$ + $\alpha_2$  (marked B) and the bright grains are Nbss (marked C).

Figure 3(b) shows the magnified image containing high Nb fields. There are areas marked as dendritic arms (DA), interdendritic channels (IC) and skeletons of Nbss. EPMA results indicate that Nb is more concentrated in the DA than in the IC. It also shows that the Nb concentration in the DA decreases from the Nbss skeleton to the periphery of the dendrites. The TEM result in Fig. 3(c) shows that the matrix is in a typically lamellar structure and the layer thickness is in the range of 70–130 nm. Figure 3(d) exhibits two kinds of O phase. One displays alternate lamellar with B2 phase, and the another shows exquixed grain. The average grain size of two kinds of O phase is in the range of 150–400 nm. The decrease of the grain size of the TiAl-Nb composite causes a clear increase of the compression yield strength based on Hall-Petch relationship between strength and grain size.

### 3.2 Fracture toughness

According to displacement-load curve shown in Fig. 4(a) and Eqs. (1) and (2), the  $P_{max}$  and  $K_Q$  of the composite are 521 N and 28.7 MPa·m<sup>1/2</sup>. Since the ASTM specifications for fracture toughness testing (E-399) were not rigorously followed in the present investigation, the measured toughness values are denoted as  $K_Q$ . The present investigation indicates that in the composite, the Nbss phase plays an important role in the fracture process. Therefore, the hardness of each phase was determined. The obtained hardnesses of the

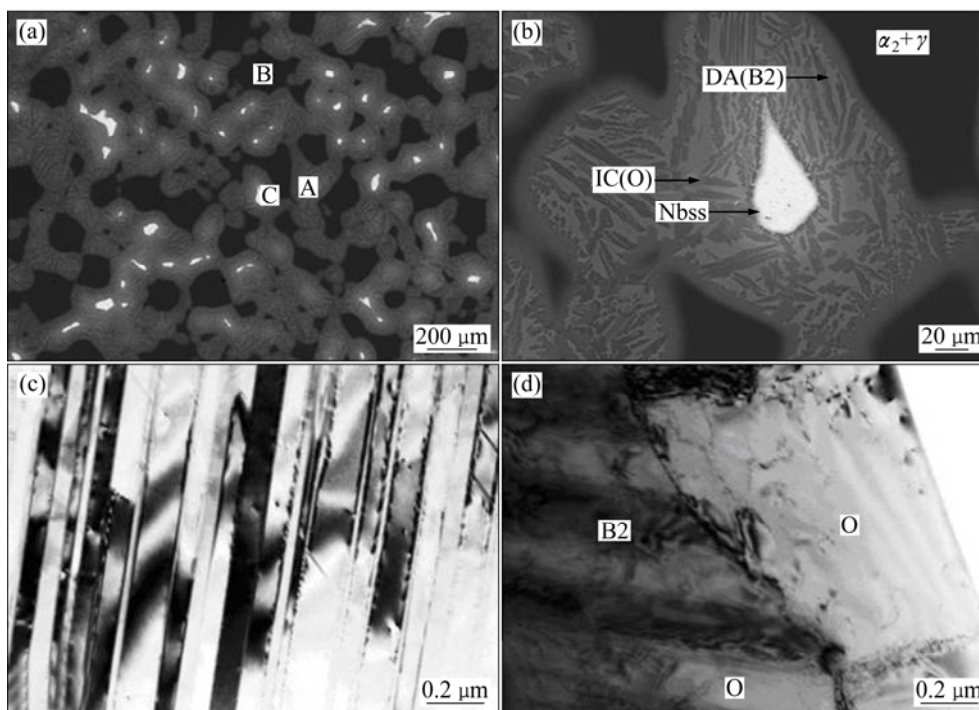
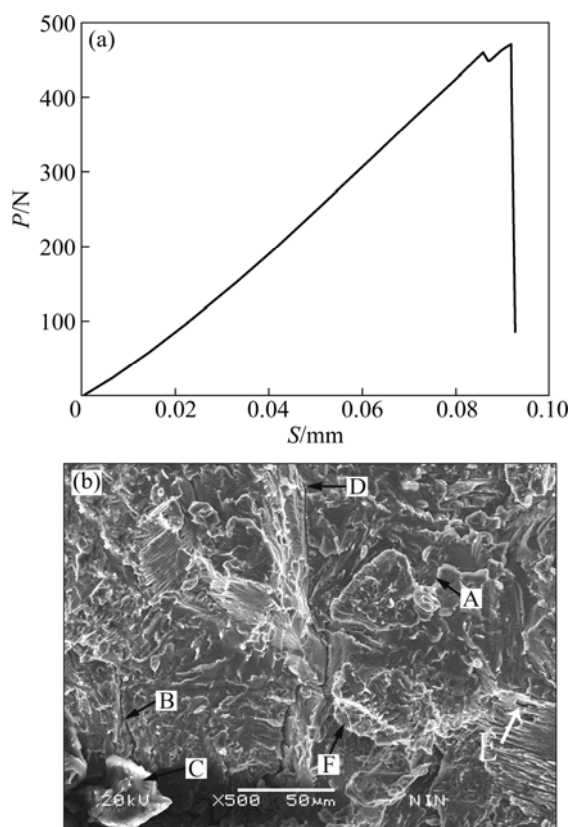


Fig. 3 EMPA (a,b) and TEM images (c,d) of composite: (a) EMPA with grain labels A, B, and C representing near Ti<sub>2</sub>AlNb, lamellar  $\alpha_2$ + $\gamma$  and Nbss, respectively; (b) Magnified EMPA showing morphology of high Nb field; (c) Bright field TEM image of matrix; (d) Bright field TEM image of O and B2 phases



**Fig. 4** Displacement—load curve (a) from three-point bending manner test and SEM image (b) of fracture surface of spark plasma sintered composite

constitute phases are summarized in Table 1. The resulted fracture toughness of the sample is much higher than that of  $\beta$  phase-containing TiAl alloys by CHEN [18], indicating that the Nbss ductile phase toughening mechanism is operative in the composite.

Fracture surface of the composite is shown in Fig. 4(b), the O phase and  $\gamma$  phase fracture in a brittle cleavage mode. However, the Nbss phase exhibits a number of different modes. These include plastic stretching and Nb/O interface decohesion, as shown by arrow A. The plastic stretching and interface decohesion will lead to an increase in the fracture toughness. The plastic stretching of Nb phase which bridges the advancing crack results in the decrease of the crack tip stress, thereby increases the toughness. Once the crack initiates, the plastic deformation of Nb phase can absorb elastic strain energy to retard the crack propagation and absorb the fracture energy in front of the cracks. The decohesion will also contribute to an increase in fracture toughness through crack deflection. The softness of the Nb phase may blunt the crack by branch and bridge, indicated by arrows B and C, which help to improve the fracture toughness. Besides, crack arrest and crack renucleation ahead of Nb indicated by arrows D and F are observed on a crack propagation path in the

composite. In addition, decohesion is observed at the interface between the Nb phase and O/B2 phase or within the lamellar phase, as indicated by the arrow E. It has been pointed out that the ductility of a phase incorporated into a brittle material and decohesion at the interface play an important role in enhancing fracture toughness. Microcracks could nucleate at the interface due to the large mismatch in mechanical properties between different phases. The hardness of B2 is lower than that of  $\gamma$  phase or O phase, as shown in Table 1. So B2 phase can be deformed more readily than  $\gamma$  or O phase. The local stress concentration at interfaces can be relieved by plastic deformation of B2 phase. So B2 phase might delay the crack nucleation and thereby increase the fracture toughness. All of the mechanisms enumerated above finally result in a large increase in toughness.

**Table 1** Density and hardness of each phase in TiAl–Nb composite sintered at 1250 °C

Density/(g·cm <sup>-3</sup> )	Hardness/GPa			
	Nbss	B2	O	$\gamma$
4.46	1.34	4.75	6.60	5.50

## 4 Conclusions

1) A TiAl–Nb composite consolidated from the mixed prealloyed TiAl powder and elemental Nb powder by SPS at 1250 °C and 50 MPa for 5 min. The density of the bulk sample was 4.46 g/cm<sup>3</sup>, equivalent to the theoretical density of the composite of 4.48 g/cm<sup>3</sup>.

2) Three different phases were observed corresponding to interpenetrating networks of Nbss, O/B2 and  $\gamma+\alpha_2$  phase. The TiAl matrix is in a typically lamellar structure and the layer thickness is in the range of 70–130 nm, while O phase exhibits two kinds of morphologies as alternative lamellar and exquixed grains with size in the range of 150–400 nm.

3) The fracture toughness of the composite is as high as 28.7 MPa·m<sup>1/2</sup>. Fractographic examination reveals that although the predominant fracture mode is cleavage, while a number of Nb grains exhibit plastic stretching and interface decohesion, leading to an increase in fracture toughness. The Nb phase plays an important role in enhancing fracture toughness by delaying crack nucleation, and causing crack deflection, branch and bridging. Various mechanisms include crack blunting, interface decohesion, crack bridge and crack branch. Considerable value of the fracture toughness of the composite was achieved.

## References

- [1] WANG Y H, LIN J P, HE Y H, WANG Y L, CHEN G L. Fabrication and SPS microstructure of Ti–45Al–8.5Nb–(W,B,Y) alloying

- powders [J]. *Intermetallics*, 2008, 16: 215–224.
- [2] GERLING R, CLEMENS H, SCHIMANSKY F P. Powder metallurgical processing of intermetallic gamma titanium aluminides [J]. *Advanced Engineering Materials*, 2004, 6: 23–38.
- [3] GERLING R, BARTELS A, CLEMENS H, KESTLER H, SCHIMANSKY F P. Structural characterization and tensile properties of a high niobium containing gamma TiAl sheet obtained by powder metallurgical processing [J]. *Intermetallics*, 2003, 51: 741–752.
- [4] CHAI L H, CHEN Y Y, ZHANG L Q, LIN J P. Effect of spark plasma sintering temperature on microstructure and mechanical properties of melt-spun TiAl alloys [J]. *Transactions of Nonferrous Metals Society of China*, 2012, 22(3): 528–533.
- [5] DING X F, ZHANG L Q, LIN J P, HE J P, YIN J, CHEN G L. Microstructure control and mechanical properties of directionally solidified TiAl–Nb alloys [J]. *Transactions of Nonferrous Metals Society of China*, 2012, 22(4): 747–753.
- [6] KRISTIC V V, NICHOLSON P S, HOAGLAND R G. Toughening of glasses by metallic particles [J]. *Journal of American Ceramic Society*, 1981, 64: 499–504.
- [7] SCHULSON E M, BARKER D R. A brittle to ductile transition in NiAl of a critical grain size [J]. *Scripta Metallurgica*, 1983, 17: 519–522.
- [8] SIGL L S, MATAGA P A, DALGLEISH B J, MCMEEKING R M, EVANS A G. On the toughness of brittle materials reinforced with a ductile phase [J]. *Acta Metallurgica*, 1988, 36: 945–953.
- [9] SIGL L S, EXNER H E. Experimental study of the mechanics of fracture in WC–Co alloy [J]. *Metallurgical and Materials Transaction A*, 1987, 18: 1299–1308.
- [10] YU J L, ZHANG K F, LI Z K, ZHENG X, WANG G F, BAI R. Fracture toughness of a hot-extruded multiphase Nb–10Si–2Fe in situ composite [J]. *Scripta Materialia*, 2009, 61: 620–623.
- [11] EMURA S, ARAOKA A, HAGIWARA M. B2 grain size refinement and its effect on room temperature tensile properties of a Ti–22Al–27Nb orthorhombic intermetallic alloy [J]. *Scripta Materialia*, 2003, 48:629–634.
- [12] ZHANG C P, ZHANG K F, WANG G F. Dependence of heating rate in PCAS on microstructures and high temperature deformation properties of  $\gamma$ -TiAl intermetallic alloys [J]. *Intermetallics*, 2010, 18: 834–840.
- [13] JABBAR H, MONCHOUX J P, THOMAS M, COURET A. Microstructure and deformation mechanisms of a G4 TiAl alloy produced by spark plasma sintering [J]. *Acta Materialia*, 2011, 59: 7574–7585.
- [14] COYRET A, MOLENAT G, GALY J, THOMAS M. Microstructure and mechanical properties of TiAl alloys consolidated by spark plasma sintering [J]. *Intermetallics*, 2008, 16: 1134–1141.
- [15] JABBAR H, COURE A, DURAND L, MONCHOUX J P. Identification of microstructural mechanisms during densification of a TiAl alloy by spark plasma sintering [J]. *Journal of Alloys and Compounds*, 2011, 509: 9826–9835.
- [16] JABBAR H, MONCHOUX J P, HOUELLIER F, DOLLE M, SCHIMANSKY F P, PYCZAK F, TOMAS M, COURT A. Microstructure and mechanical properties of high niobium containing TiAl alloys elaborated by spark plasma sintering [J]. *Intermetallics*, 2010, 18: 2312–2321.
- [17] CAO R, LEI M X, CHEN J H, ZHANG J. Effects of loading rate on damage and fracture behavior of TiAl alloys [J]. *Materials Science and Engineering A*, 2007, 465: 183–193.
- [18] CHEN Y Y, NIU H Z, KONG F T, XIAO S L. Microstructure and of fracture toughness of a  $\beta$  phase containing TiAl alloy [J]. *Intermetallics*, 2011, 19: 1405–1410.

## 等离子电火花烧结 TiAl–Nb 复合材料的显微组织与断裂韧性

杨鑫<sup>1,2</sup>, 奚正平<sup>2</sup>, 刘咏<sup>1</sup>, 汤慧萍<sup>2</sup>, 胡可<sup>3</sup>, 贾文鹏<sup>2</sup>

1. 中南大学 粉末冶金国家重点实验室, 长沙 410083;
2. 西北有色金属研究院 金属多孔材料国家重点实验室, 西安 710016;
3. 华南理工大学 金属材料近净成形国家工程中心, 广州 510641

**摘要:** 将钛铝预合金粉末和铌粉按照摩尔比 9:1 混合均匀, 再采用等离子电火花烧结技术在 1250 °C、50 MPa 下烧结 5 min 制备细晶钛铝基复合材料。采用 X 射线衍射、电子扫描、透射以及电子探针探讨烧结样品中显微组织、相成分的分布及晶粒度。结果表明: 合金的显微组织主要由大量的层片  $\gamma$  相、O 相、Nbss(Nb 固溶相)以及 B2 相组成; 室温烧结样品的断裂韧性高达 28.7 MPa·m<sup>1/2</sup>, 韧性铌固溶相在裂纹尖端以塑性延伸的方式吸收断裂能, 从而提高了合金的断裂韧性; B2 相以也会促进裂纹的桥联和分叉。对合金各相的显微硬度也进行了测试。

**关键词:** TiAl–Nb 复合材料; 断裂; 等离子电火花烧结; 粉末冶金; 断裂韧性; 断裂能; 裂纹扩展

(Edited by YANG Hua)